In Situ Insights into the Nucleation and Growth Mechanisms of Gold Nanoparticles on Tobacco Mosaic Virus

Cora Moreira da Silva, Nathaly Ortiz-Peña, Leïla Boubekeur-Lecaque, Jakub Dušek, Tomáš Moravec, Damien Alloyeau, Nguyêt-Thanh Ha-Duong

In Situ Insights into the Nucleation and Growth Mechanisms of Gold Nanoparticles on Tobacco Mosaic Virus

Cora Moreira Da Silva,[†] Nathaly Ortiz-Peña,[‡] Leïla Boubekeur-Lecaque,[†] Jakub Dušek,[¶] Tomàš Moravec,[¶] Damien Alloyeau,[*,‡] and Nguyêt-Thanh Ha-Duong[*,†]

[†]*Université Paris Cité, ITODYS, CNRS, F-75013 Paris, France*

[‡]*Université Paris Cité, CNRS, Laboratoire Matériaux et Phénomènes Quantiques, 75013 Paris, France*

[¶]*Institute of Experimental Botany of the Czech Academy of Sciences, Rozvojová 263, Prague 6, 160 00, Czech Republic*

E-mail: damien.alloyeau@u-paris.fr; thanh.haduong@u-paris.fr

Abstract

Biotemplated syntheses have emerged as an efficient strategy to control the assembly of metal nanoparticles (NPs) and generate promising plasmonic properties for sensing or biomedical applications. However, understanding the nucleation and growth mechanisms of metallic nanostructures on biotemplate is an essential prerequisite to developing well-controlled nanotechnologies. Here, we used liquid cell Transmission Electron Microscopy (TEM) to reveal how the formation kinetics of gold NPs affects their size and density on Tobacco Mosaic Virus (TMV). These *in situ* insights are used as a guideline to optimize bench-scale synthesis with the possibility to homogenize the coverage and tune the density of gold NPs on TMV. In line with *in situ* TEM observations, fluorescence spectroscopy confirms that the nucleation of NPs occurs on the virus

capsid rather than in solution. The proximity of gold NPs on TMV allows shifting the plasmonic resonance of the assembly in the biological window.

KEYWORDS: *Biomineralization, nano-bio-hybrid, plant virus, in situ liquid transmission electron microscopy, plasmonic resonance*

Controlling the three-dimensional spatial distribution of plasmonic nanostructures at the nanoscale has been a major challenge to developing efficient nanotechnologies for biomedical and sensing applications.[1–4] Indeed, the proximity of Au nanoparticles (NPs) generates plasmonic hot spots with a high enhancement factor, and a red-shift and broadening of the plasmon resonance band leading to better light-response sensitivity in the biological window (*i.e.* Near Infra-Red (NIR)).[5,6] In that regard, biomolecules have been used as biotemplate to design uniform nanostructure assemblies, thanks to the functional groups on their surface which allow the NP organizations by chemical conjugation or biomineralization. 1D and 2D Au NP assemblies were formed on microtubules proteins,[7] amyloid fibers,[8] and DNA origami.[9,10] DNA origami also offered the possibility to fabricate 3D NP superlattices or large-size nanoarchitectures.[11–13] More recently, viruses have been used as scaffolds in nano-biotechnology, because of their variety in size, symmetry and shape, their low cost of production and their ability to self-assemble.[14–16] These virus-based approaches allow the fabrication of nanomaterials with many applications, such as biomedicine, catalysis and energy storage.[17–21] Cowpea mosaic virus has been decorated by quantum dots for fluorescence applications,[22] and gold NPs for SERS and electronic nanosensors.[23–25] Recently, we have also obtained in-solution SERS sensors by grafting Au NPs onto Turnip yellow mosaic virus capsid.[26]

Metal NPs assemblies can also be directly mineralized on viruses by reducing aqueous metal salts. For example, Barley stripe mosaic virus has been decorated by Pd and Au,[27] and the nucleation and growth of gold nanocrystals on bacteriophage P22 capsid has been studied

using *ex situ* characterization methods.[28] Tobacco mosaic virus is one of the most exploited plant viruses, due to its ease of production, physical properties, stability and structure.[29,30] TMV is a helical, rod-shaped virus of 300 nm long. The diameter of its capsid is 18 nm, and its inner cavity 4 nm.[31,32] The Blum's team succeeded to assemble gold and silver NPs as nanoring using this remarkable biotemplate[33,34] and the mineralization of gold NPs in its inner cavity[35] and at the surface of its capsid was also demonstrated.[36,37]

As with bottom-up synthesis, the nucleation and growth mechanisms of metal NPs on viruses are simultaneously driven by kinetic and thermodynamic effects. Indeed, the physico-chemical properties of virus capsid can affect the reduction, adsorption, nucleation and growth rates of metals and the equilibrium shape of NPs. Additionally, the competition and interplay between heterogenous (*i.e.* on viruses) and homogenous (*i.e.* in solution) formation processes can also affect the density, size and shape of NPs on viruses. Given the complexity of the atomic-scale processes occurring at these soft-hard materials interfaces, *in situ* studies are necessary to better understand biotemplated synthesis. On the one hand, UV-Vis spectroscopy is often employed to extract information on the morphology and organization of metal NPs during their formation.[37–39] X-ray scattering approaches combined with data modeling can be also used, as evidenced by the SAXS study of Michael T. Harris's group on the growth of gold and palladium onto TMV.[40] Although essential, such averaged and indirect *in situ* measurements provide only a partial view of the nucleation and growth processes. On the other hand, liquid cell transmission electron microscopy (LCTEM) has become a very popular *in situ* technique to directly visualize the formation of metal NPs in solution with the unique possibility to follow the nucleation and growth processes of individual NPs in reactive media of controlled composition and temperature.[41–43] Additionally, LCTEM has also emerged as a complementary approach to cryo-TEM to study biomaterials in their native state.[44] The growth of metallic layers at the surface of bacteria[45] and extracellular vesicles[46,47] has already been investigated either to improve the contrast of biomaterials or to understand mineralization in biofilms. Nevertheless, the controlled biotemplated syn-

thesis of plasmonic nano-assemblies on viruses remains unexplored with LCTEM.

Here we combined LCTEM, UV-Vis and absorption and emission spectroscopies to investigate the formation mechanisms of gold NPs at the surface of TMV. Our multi-scale approach highlights the key role of reaction kinetics on the nucleation and growth processes and allows designing optimized synthesis protocol with a more homogenous cover rate and a higher NP density.

Most of the publications in the literature propose biomineralization syntheses divided into cycles of successive additions of metal complex ($HAuCl_4$) and reductant in acidic media to favor electrostatic bounding between the gold precursors and the outer surface of TMV.[36,37] Therefore, LCTEM observations were performed in a solution containing intact TMV virions (0.2 $mg.mL^{-1}$) and $HAuCl_4$ (1 mM) diluted in acetic acid (acetic acid 5 %, pH = 2.4) incubated for two hours including 15 minutes in a sonification bath prior loading in the TEM liquid cell. A solution of gold complex (1 mM) dissolved in acetic acid was continuously flowing in the liquid cell during TEM observations. The reduction reaction was driven by radiolysis which allows controlling the formation kinetics of metal NPs with the electron dose rate, here controlled by changing the magnification.

Indeed, as the steady-state concentration of reducing agents (mainly e^-_{aq} and $H^{\cdot}$)[48] produced by radiolysis increases with $\dot{d}$,[49] liquid cell TEM has been deeply used to study kinetic effects on the nucleation and growth processes of inorganic nanomaterials.[50–53] Here, LCTEM experiments were performed at three different $\dot{d}$: 0.14 e^-/A^2s (Figures 1a-d), 0.55 e^-/A^2s (Figures 1e-h) and 2.2 e^-/A^2s (Figures 1i-l) and image processing was used to quantify the total amount of gold (Figure 2a) and the NP density (Figure 2b) on the viruses over the acquisition time.

Despite many studies on the biotemplated synthesis of NPs on virus capsids, some aspects of the nucleation mechanisms are still unclear: do the *nuclei* form in solution and then attach to the surface of the viruses by diffusion, or do they form directly on the surface of the virus?

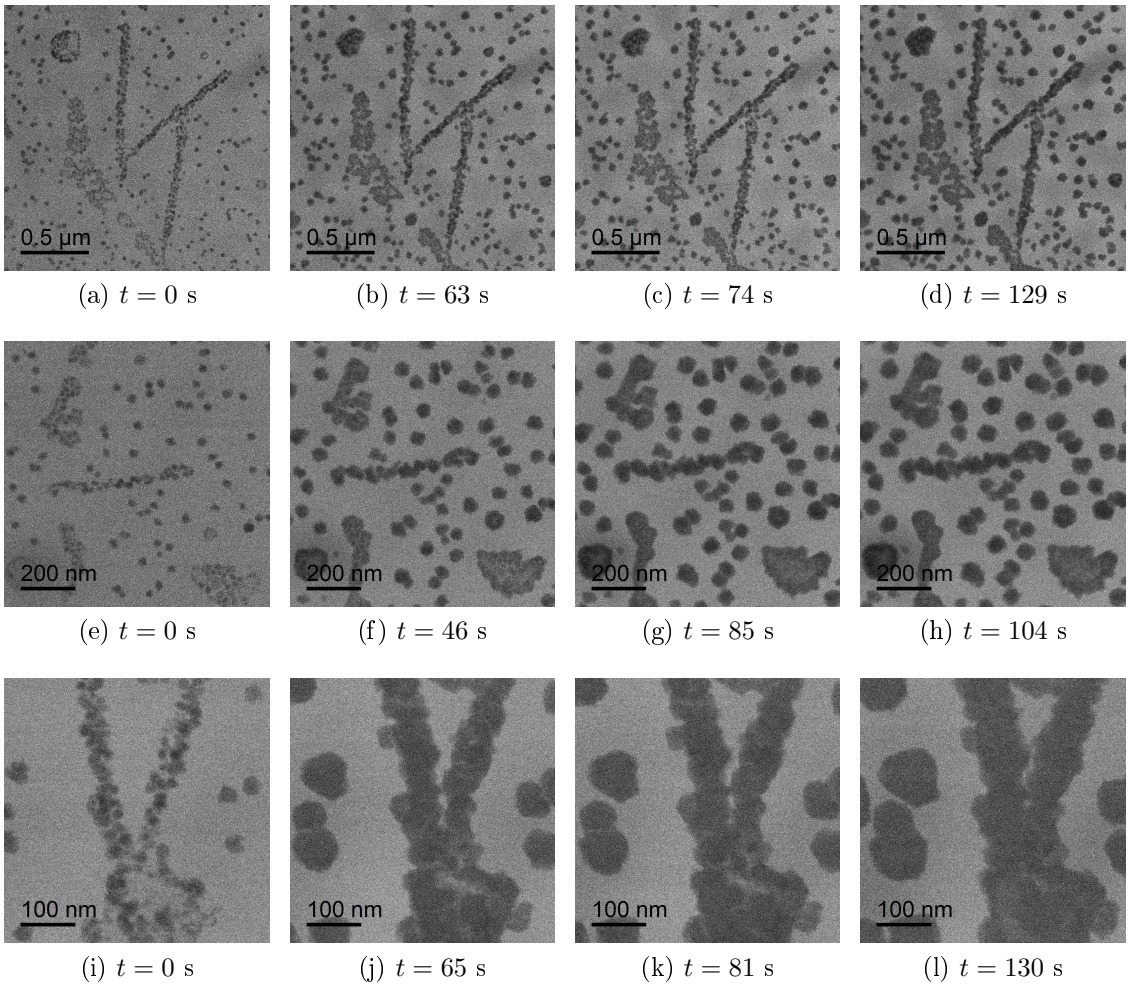

(a) $t = 0$ s (b) $t = 63$ s (c) $t = 74$ s (d) $t = 129$ s

(e) $t = 0$ s (f) $t = 46$ s (g) $t = 85$ s (h) $t = 104$ s

(i) $t = 0$ s (j) $t = 65$ s (k) $t = 81$ s (l) $t = 130$ s

Figure 1: LCTEM image series of gold NP growth, at different electron dose rates: (a)-(d) $\dot{d}_1 = 0.14$ e$^-$/A^{2}s, (e)-(h) $\dot{d}_2 = 0.55$ e$^-$/A^{2}s and (i)-(l) $\dot{d}_3 = 2.2$ e$^-$/A^{2}s. The acquisition time is indicated below each image.

Or both homogenous and heterogenous nucleation occur simultaneously? At first, our direct nanoscale observations allow identifying the preferential nucleation sites of gold NPs in the reaction media. Indeed, at all dose rates, many nanoparticles nucleate on the virus capsid in the very first moment of TEM observations. As previously reported,[50–53] NPs can also form on the SiN membrane, but the NP density on the liquid cell window is several orders of magnitude lower than on TMV (Figure S1 of SI) and no diffusion of NPs from the solution to the viruses is observed. It is worth noting that the isoelectric point (pI) of the TMV capsid has been estimated to be between 3.5 and 4.6.[54,55] The outer surface is positively charged at

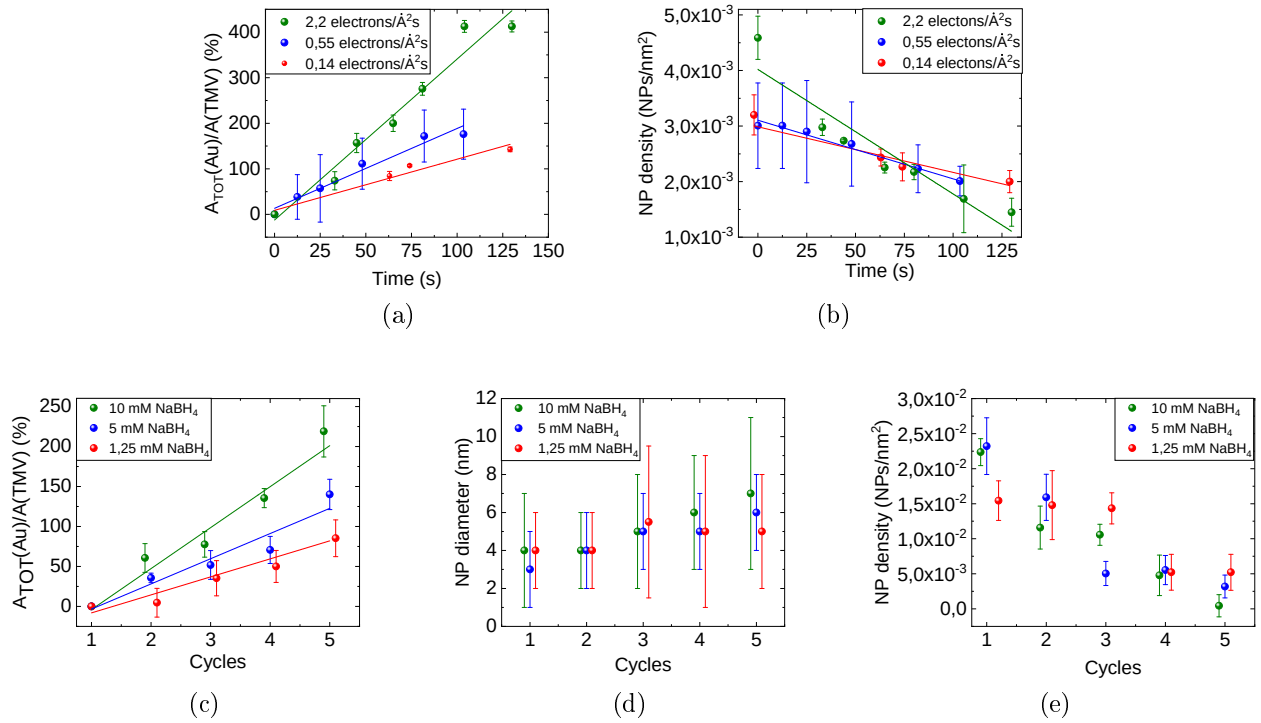

Figure 2: Quantitative analysis of LCTEM experiments: effect of the electron dose rate on (a) the time evolution of the ratio between the total projected surface of the nanostructured gold layer and the projected surface of TMV, (b) the time evolution of Au NP density on TMV (in red $\dot{d}_1 = 0.14$ e$^-$/A^{2}s, in blue $\dot{d}_2 = 0.55$ e$^-$/A^{2}s, in green $\dot{d}_3 = 2.2$ e$^-$/A^{2}s). Quantitative *ex situ* TEM analysis of beaker experiments. Effect of the $NaBH_4$ concentration on (c) the evolution of the ratio between the total projected surface of the nanostructured gold layer and the projected surface of TMV per cycle, (d) NP size on TMV evolution per cycle, (e) NP density on TMV evolution per cycle (in red $[NaBH_4] = 1.25$ mM, in blue $[NaBH_4] = 5$ mM, in green $[NaBH_4] = 10$ mM).

the final pH (pH $\sim$ 3). Indeed, the accessible amino acids on the outer surface are mostly arginine (R46, 61, 141 and 134, pKa of side chain = 12.1), Lys (K53, pKa = 10.53), and Asp (D19, 64, pKa = 3.90),[30,36,56] whereas, the inner surface is composed with glutamic acids (E97 and E106, pKa = 4.07).[30,56] Thus, our *in situ* TEM observations confirm that in acidic conditions (pH $\sim$ 3), the positively charged outer surface of the virus[36] attracts gold precursors and creates very stable nucleation sites. The absence of NPs within the virus confirms that the neutral inner surface of the capsid does not favor the encapsulation of $AuCl_4^-$. We note that NPs are systematically observed on the very first images of the viruses

which prevent observing directly the nucleation events. The burst of nucleation is the nucleation is shorter than the acquisition time of the first image because the aqueous electrons produced by water radiolysis are very reactive reducing agent. The formation of NPs could possibly be driven by the capsid surface during the incubation time of TMVs with gold precursor solution.[37] However, *ex situ* TEM images acquired after the incubation step show that no particles formed on the virus without the introduction of reducing agents (Figure S2 of SI). Moreover, as the NP density on the first image of viruses rises substantially with $\dot{d}$ (Figure 2b) the nucleation is obviously beam induced and the nucleation rate increases with the concentration of reducing agents. Once the NPs are formed in the very first seconds of observation, they grow first by monomer attachment and by coalescence when they get in contact with each other, leading to a decrease of NP density over time (Figure 2b). For all experiments, the ratio between the total projected surface of the nanostructured gold layer and the projected surface of TMV increases linearly with time (Figure 2a). As expected, the higher $\dot{d}$, the faster the growth processes and consequently NP density drops much more rapidly in high $\dot{d}$ conditions.

To confirm the effects of reaction kinetics on NP size and density, we performed bench-scale biotemplated syntheses in the same reaction media. The reduction of metal complexes was generated by 5 sequential injections of $NaBH_4$ and $HAuCl_4$. We performed three syntheses with different $NaBH_4$ concentrations (10 mM, 5 mM and 1.25 mM, pH = 9.8) but constant over the 5 reduction cycles. *Ex situ* TEM (Figures 3a-c and S3 of SI) was used to quantify the total projected surface of the nanostructured gold layer normalized by the projected surface of TMV (Figure 2c), the NP size (Figure 2d) and density on TMV (Figure 2e) after each reduction cycle. In all syntheses, the NP density is maximum after the first reduction step and decreases over the subsequent cycles (Figure 2e), while the mean size of NPs increases (Figure 2d). All the TMV are homogenously covered during the synthesis (Figures 3a-c and S3 of SI). In line with *in situ* observations, the great majority of NPs are formed after the first cycle and coalescence is obviously involved together with monomer attachment in

the growth mechanisms. We also clearly see that the $NaBH_4$ concentrations have the same effects that $\dot{d}$ in the *in situ* experiments: a high concentration of reducing agents boosts the nucleation and growth rates.

It is also important to discuss the differences between the *in situ* and bench-scale syntheses. Even at a low dose rate, the growth kinetics of gold NPs on the viruses is faster in the TEM liquid cell than in the beaker. As seen in Figure 1, in the first seconds of LCTEM observation, isolated NPs are formed as in the *ex situ* experiments using $NaBH_4$ as a reducing agent (Figures 3a-c and S3). However, at a longer time, the radiolysis-driven growth and coalescence processes lead to bigger NPs with a lower density on the viruses than the nanohybrid materials observed by *ex situ* TEM after five injection cycles. Several factors can explain the different growth kinetics between the *in situ* and *ex situ* syntheses. At first, the aqueous electrons produced by radiolysis are stronger reducing agents than $NaBH_4$. Moreover, the growth occurs only in the irradiated area of the liquid cell, while NP formation occurs in the whole solution volume in the bench-scale syntheses. Finally, the injection of the gold precursor is sequential in *ex situ* syntheses while a continuous flow of gold precursors is injected into the liquid cell during TEM observations. Thus, the faster and continuous growth kinetic in the liquid cell leads more rapidly to the formation of a quasi-continuous layer of gold via the growth and coalescence of NPs on the viruses. Similar nanohybrid materials can be obtained at the bench scale after 15 injection cycles (Figure S4).

These *ex situ* and *in situ* TEM investigations allow evaluating the effects of the reaction kinetics on the nucleation and growth mechanisms and the resulting size and density of NPs with the view to design optimized synthesis protocols. On the one hand, the best parameter to control NP size remains the number of reducing cycles. If the growth dynamics increase with the concentration of reducing agent (Figure 2d), the size distributions of NPs measured at various $NaBH_4$ concentrations always overlap because the size polydispersity is always between 50 and 80 %. On the other hand, the reaction kinetics provides more precise control over the NP density since it allows tuning the amplitude of the nucleation burst and the

coalescence phenomena. To obtain TMV with high-density coverage, we must increase the reduction rate of metal precursors at the nucleation stage and reduce it during the growth phase. We have applied this strategy by using a $NaBH_4$ concentration of 25 mM during the first reduction cycle and reducing it to 5 mM in the following cycles and we performed TEM analysis after each cycle (Figures 3d-f and S5 of SI). As shown in Figure 4, twice higher density of NPs with similar size can be obtained compared to syntheses with homogenous $NaBH_4$ concentration (5 mM) at each cycle.

It is worth noting that the incubation step, during which TMV and gold precursors are mixed, can also influence the nucleation and growth processes. Indeed, reducing the incubation time to 15 min without sonification period, corresponding to the synthesis conditions of Bromley *et al.*,[37] drastically modifies the evolution of NP density and the monodispersity of NP size over 5 reduction cycles with homogenous $NaBH_4$ concentrations (5 mM) (Figure 4a). Without sonification, the TMV are more aggregated which reduces the accessibility for gold precursors. Consequently, NP nucleation does not occur on all TMV at the beginning of the synthesis and many viruses are naked or partially covered after the first cycles (Figures 3g-i). The averaged NP density increases with the number of cycles because the proportion of covered viruses rises. This inhomogeneous nucleation phase lead to lower NP density and less uniform coverage across TMVs.

HRTEM analysis revealed that gold NPs on TMV are mostly multi-twinned nanostructures with a lattice parameter of (0.406 ± 0.003) nm (Figure S6 of SI). As the size of NPs increases with the number of reduction cycles, the distance between NPs decreases. As illustrated in Figure S7 of SI, the number of NPs in contact or near contact with each other increases with the number of cycles. This proximity induces plasmonic interactions resulting in a broader plasmonic band with a red-shift of 10 nm compared to the plasmonic band of Au NPs in solution (Figure 5a). Note that the addition of a biocompatible surface coating material (dextran) only at the end of the last cycle enlarges ever further the plasmonic band of the

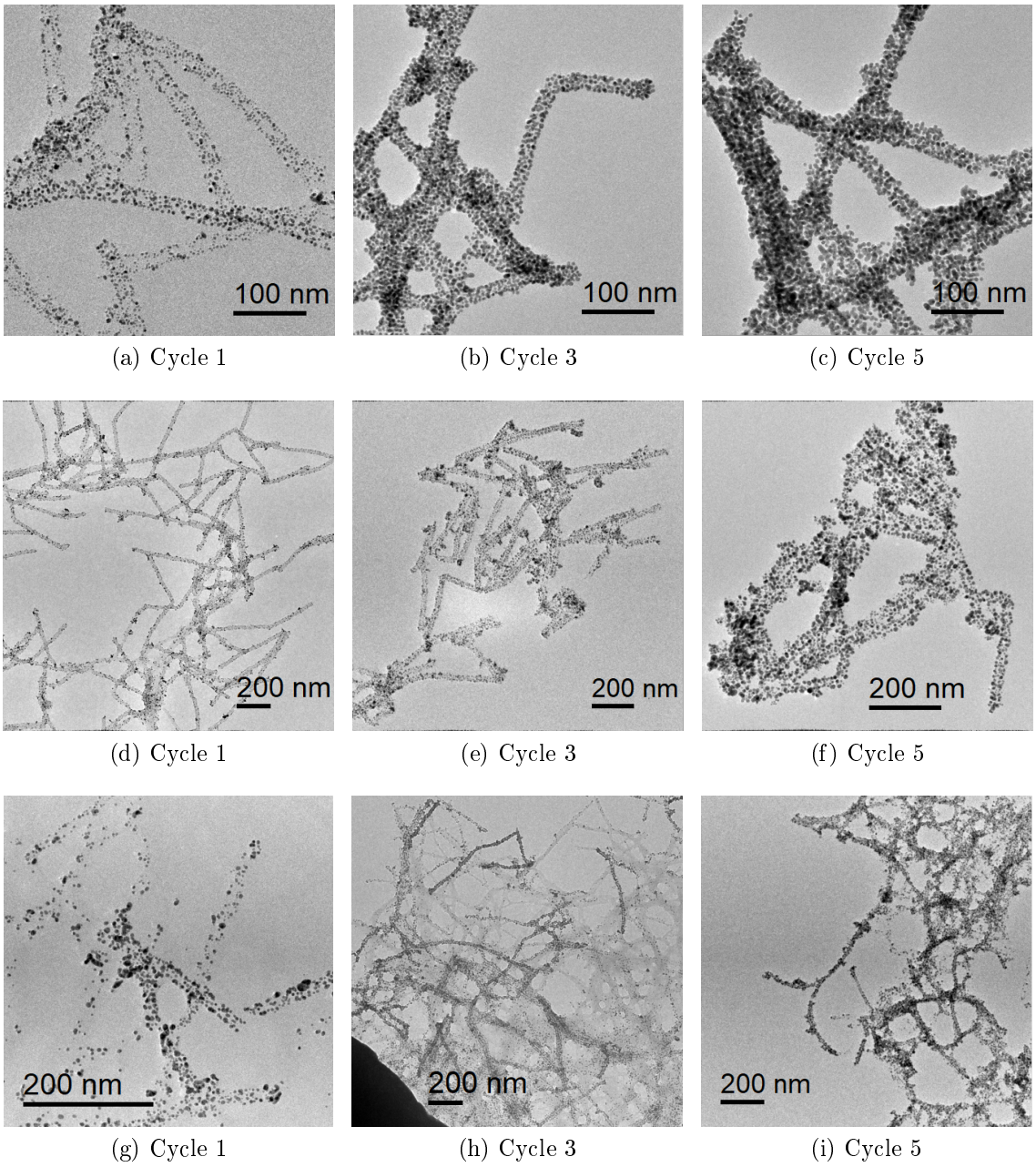

(a) Cycle 1 (b) Cycle 3 (c) Cycle 5

(d) Cycle 1 (e) Cycle 3 (f) Cycle 5

(g) Cycle 1 (h) Cycle 3 (i) Cycle 5

Figure 3: TEM images of gold NPs after reduction cycles 1, 3 and 5 for the following synthesis conditions (TEM images after all cycles can be seen in Figure S5 in SI): (a)-(c) 5 cycles with constant $[NaBH_4]_{1-5} = 5$ mM, with 2 h incubation time including 15 min in ultrasonic bath prior the first cycle, (d)-(f) first cycle with $[NaBH_4]_1 = 25$ mM and $[NaBH_4]_{2-5} = 5$ mM at cycles 2-5, with 2 h incubation time including 15 min in ultrasonic bath prior the first cycle, (g)-(j) 5 cycles with constant $[NaBH_4]_{1-5} = 5$ mM, with 15 min incubation time prior the first cycle (no ultrasonication).

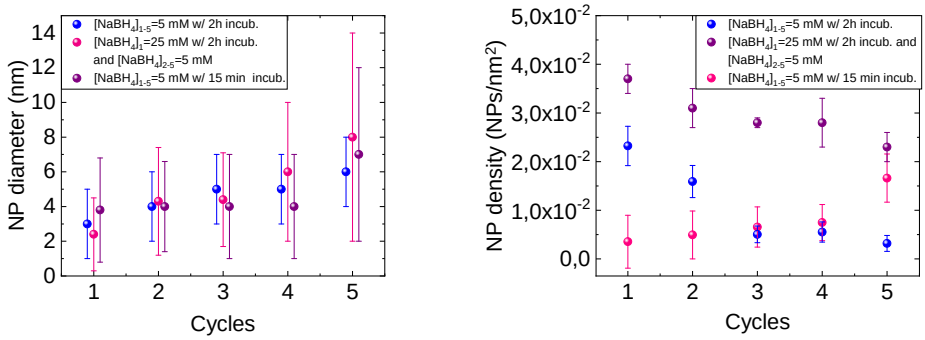

(a) (b)

Figure 4: (a) NP size and (b) NP density on TMV measured on the TEM images seen in Figures 3 and S5 of SI. Blue data points: 5 cycles with constant $[NaBH_4]_{1-5} = 5$ mM, with 2 h incubation time including 15 min in ultrasonic bath prior the first cycle. Pink data points: first cycle with $[NaBH_4]_1 = 25$ mM and $[NaBH_4]_{2-5} = 5$ mM for cycle 2-5, with 2 h incubation time including 15 min in ultrasonic bath prior the first cycle. Purple data points: 5 cycles with constant $[NaBH_4]_{1-5} = 5$ mM, with 15 min incubation time prior to the first cycle (no ultrasonication).

colloidal solution (Figure 5a) and allows increasing the dispersity and stability of metalized virions. This opens up the possibility to use such nano-bio-hybrid materials in biological applications.

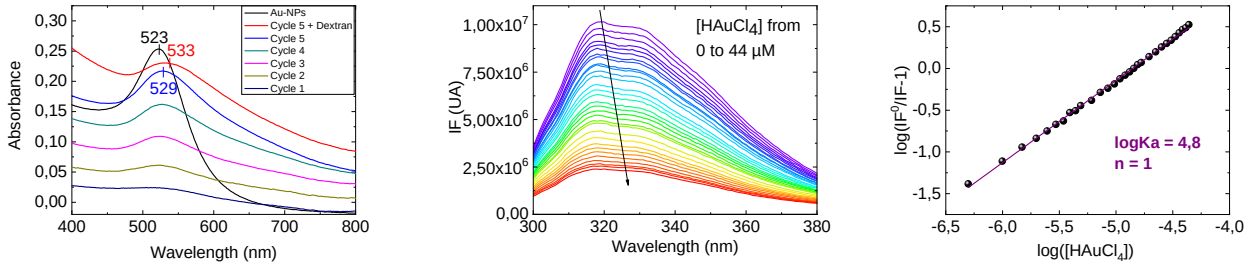

(a) (b) (c)

Figure 5: (a) UV-Vis spectra of 10 nm Au NPs in solution, NPs on TMV after each cycle and after dextran was added at the end of the synthesis. (b) fluorescence emission spectra recorded at 25 °C, between 300 – 380 nm, on a Fluorolog spectrophotometer equipped with external thermostated water-bath circulation, at $\lambda_{excitation} = 280$ nm with different concentrations of $HAuCl_4$ at pH 2.4 and (c) Modified Stern Volmer curve obtained by the equation 1.

We have also performed fluorescence experiments to evaluate the interaction between the

gold complexes and the virus surface in acidic conditions (pH 2.4). Fluorescence spectra of a TMV solution recorded with an increasing concentration of $HAuCl_4$ (Figure 5b) were analyzed using a modified Stern Volmer model (equation 1) to measure an apparent affinity constant value of $10^{4.8}$ (Figure 5c).[57] This result confirms an interaction between the gold complex and the virus surface that could explain the preferential nucleation of NPs on the viruses measured by liquid cell TEM.

$$log(\frac{IF^0}{IF} - 1) = logK_a + n.log[HAuCl_4] \quad (1)$$

By combining LCTEM and fluorescence spectroscopy, the nucleation and growth mechanisms of gold NPs on TMV were unequivocally identified according to (1) interaction between the gold complex and the virus' surface, (2) NP nucleation directly on the virus' surface, (3) particles grow by monomer attachment and (4) coalescence when NPs gets in contact. Direct *in situ* TEM observations at the single virus level revealed how the reaction kinetics affects the nucleation and growth rates of NPs, which allows designing synthesis protocols with reduction cycles of different intensities to enhance the density of NPs on TMV. The accessibility of gold precursors to the TMV surface during the incubation time can also affect the uniformity of the NP coverage. The high density of NPs on the viruses enables the red-shift of the light absorption. Further studies improving the NP coupling on TMV would allow the use of these solution-stable nano-bio-hybrids for biomedical applications. More generally, this work highlights the interest in directly visualizing the nucleation and growth phenomena in complex environments to deepen our knowledge on the nano/bio interfaces and to optimize our synthesis strategies of nanoassemblies on biotemplates.

Acknowledgement

ANR (Agence Nationale de la Recherche) and CGI (Commissariat à l'Investissement d'Avenir)

are gratefully acknowledged for their financial support of this work through Labex SEAM (Science and Engineering for Advanced Materials and devices), ANR-10-LABX-0096 and ANR-18-IDEX-0001.

T. M. and J. D. were supported by the European Regional Development Fund-Project "Centre for Experimental Plant Biology" (grant number CZ.02.1.01/0.0/0.0/16_0190000738) from the Ministry of Education, Youth and Sports of CR.

Supporting Information Available

TMV extraction, nanoparticles synthesis on TMV, conventional TEM characterization, liquid TEM experiments, absorption and emission spectroscopy and additional TEM images are presented and detailed in the Supporting Information file.

References

(1) Lee, S.; Sim, K.; Moon, S. Y.; Choi, J.; Jeon, Y.; Nam, J.-M.; Park, S.-J. Controlled assembly of plasmonic nanoparticles: from static to dynamic nanostructures. *Advanced Materials* **2021**, *33*, 2007668.

(2) Vila-Liarte, D.; Kotov, N. A.; Liz-Marzán, L. M. Template-assisted self-assembly of achiral plasmonic nanoparticles into chiral structures. *Chemical Science* **2022**, *13*, 595–610.

(3) Tim, B.; Błaszkiewicz, P.; Kotkowiak, M. Recent advances in metallic nanoparticle assemblies for surface-enhanced spectroscopy. *International Journal of Molecular Sciences* **2022**, *23*, 291.

(4) Chen, J.; Gong, M.; Fan, Y.; Feng, J.; Han, L.; Xin, H. L.; Cao, M.; Zhang, Q.; Zhang, D.; Lei, D., et al. Collective plasmon coupling in gold nanoparticle clusters for highly efficient photothermal therapy. *ACS Nano* **2022**, *16*, 910–920.

(5) Huang, W.; Qian, W.; Jain, P. K.; El-Sayed, M. A. The effect of plasmon field on the coherent lattice phonon oscillation in electron-beam fabricated gold nanoparticle pairs. *Nano Letters* **2007**, *7*, 3227–3234.

(6) Litti, L.; Meneghetti, M. Predictions on the SERS enhancement factor of gold nanosphere aggregate samples. *Physical Chemistry Chemical Physics* **2019**, *21*, 15515–15522.

(7) Zhou, J. C.; Gao, Y.; Martinez-Molares, A. A.; Jing, X.; Yan, D.; Lau, J.; Hamasaki, T.; Ozkan, C. S.; Ozkan, M.; Hu, E.; Dunn, B. Microtubule-based gold nanowires and nanowire arrays. *Small* **2008**, *4*, 1507–1515.

(8) Mavlankar, N. A.; Awasthi, A. K.; Ralhan, J.; Pal, A. Amyloid-inspired Peptide Self-assembly/Disassembly as intervened by Gold Nanoparticles and Polydopamine Coating to Dictate Spatiotemporal Organization. *Chem. Nano. Mat.* **2022**, e202200368.

(9) Ohya, Y.; Miyoshi, N.; Hashizume, M.; Tamaki, T.; Uehara, T.; Shingubara, S.; Kuzuya, A. Formation of 1D and 2D gold nanoparticle arrays by divalent DNA-gold nanoparticle conjugates. *Small* **2012**, *8*, 2335–2340.

(10) Yao, Y.; Wei, Y.; Chen, S. Size effect of the surface energy density of nanoparticles. *Surface Science* **2015**, *636*, 19–24.

(11) Yin, J.; Xie, M.; Wang, J.; Cui, M.; Zhu, D.; Su, S.; Fan, C.; Chao, J.; Li, Q.; Wang, L. Gold-Nanoparticle-Mediated Assembly of High-Order DNA Nano-Architectures. *Small* **2022**, *18*, 2200824.

(12) Pothukuchi, R. P.; Singh, U.; Bhatia, D.; Radhakrishna, M. Controlled 3D assembly and stimuli responsive behavior of DNA and peptide functionalized gold nanoparticles in solutions. *Physical Chemistry Chemical Physics* **2022**, *24*, 19552–19563.

(13) Schreiber, R.; Santiago, I.; Ardavan, A.; Turberfield, A. J. Ordering Gold Nanoparticles with DNA Origami Nanoflowers. *ACS Nano* **2016**, *10*, 7303–7306.

(14) Zhang, Y.; Dong, Y.; Zhou, J.; Li, X.; Wang, F. Application of plant viruses as a biotemplate for nanomaterial fabrication. *Molecules* **2018**, *23*, 2311.

(15) Lee, S.-Y.; Lim, J.-S.; Harris, M. T. Synthesis and application of virus-based hybrid nanomaterials. *Biotechnology and Bioengineering* **2012**, *109*, 16–30.

(16) Alloyeau, D.; Stephanidis, B.; Zhao, X.; Larquet, E.; Boisset, N.; Ricolleau, C. Biotemplated synthesis of metallic nanoclusters organized in tunable two-dimensional superlattices. *The Journal of Physical Chemistry C* **2011**, *115*, 20926–20930.

(17) Capek, I. Viral nanoparticles, noble metal decorated viruses and their nanoconjugates. *Advances in Colloid and Interface Science* **2015**, *222*, 119–134.

(18) Culver, J. N.; Brown, A. D.; Zang, F.; Gnerlich, M.; Gerasopoulos, K.; Ghodssi, R. Plant virus directed fabrication of nanoscale materials and devices. *Virology* **2015**, *479*, 200–212.

(19) Li, F.; Wang, Q. Fabrication of nanoarchitectures templated by virus-based nanoparticles: strategies and applications. *Small* **2014**, *10*, 230–245.

(20) Liu, B.; Ren, W.; Li, S.; Liu, C.; Cheng, H.-M. High temperature selective growth of single-walled carbon nanotubes with a narrow chirality distribution from a CoPt bimetallic catalyst. *Chemical Communications* **2012**, *48*, 2409.

(21) Petrescu, D. S.; Blum, A. S. Viral-based nanomaterials for plasmonic and photonic materials and devices. *Wiley Interdisciplinary Reviews: Nanomedicine and Nanobiotechnology* **2018**, *10*, e1508.

(22) Blum, A. S.; Soto, C. M.; Wilson, C. D.; Whitley, J. L.; Moore, M. H.; Sapsford, K. E.; Lin, T.; Chatterji, A.; Johnson, J. E.; Ratna, B. R. Templated self-assembly of quantum

dots from aqueous solution using protein scaffolds. *Nanotechnology* **2006**, *17*, 5073–5079.

(23) Blum, A. S.; Soto, C. M.; Sapsford, K. E.; Wilson, C. D.; Moore, M. H.; Ratna, B. R. Molecular electronics based nanosensors on a viral scaffold. *Biosensors and Bioelectronics* **2011**, *26*, 2852–2857.

(24) Soto, C. M.; Blum, A. S.; Wilson, C. D.; Lazorcik, J.; Kim, M.; Gnade, B.; Ratna, B. R. Separation and recovery of intact gold-virus complex by agarose electrophoresis and electroelution: Application to the purification of cowpea mosaic virus and colloidal gold complex. *Electrophoresis* **2004**, *25*, 2901–2906.

(25) Lebedev, N.; Griva, I.; Dressick, W. J.; Phelps, J.; Johnson, J. E.; Meshcheriakova, Y.; Lomonossoff, G. P.; Soto, C. M. A virus-based nanoplasmonic structure as a surface-enhanced Raman biosensor. *Biosensors and Bioelectronics* **2016**, *77*, 306–314.

(26) Nguyen, H. A.; Jupin, I.; Decorse, P.; Lau-Truong, S.; Ammar, S.; Ha-Duong, N. T. Assembly of gold nanoparticles using turnip yellow mosaic virus as an in-solution SERS sensor. *RSC Advances* **2019**, *9*, 32296–32307.

(27) Adigun, O. O.; Retzlaff-Roberts, E. L.; Novikova, G.; Wang, L.; Kim, B.-S.; Ilavsky, J.; Miller, J. T.; Loesch-Fries, L. S.; Harris, M. T. BSMV as a biotemplate for palladium nanomaterial synthesis. *Langmuir* **2017**, *33*, 1716–1724.

(28) Zhou, Z.; Bedwell, G. J.; Li, R.; Palchoudhury, S.; Prevelige, P. E.; Gupta, A. Pathways for gold nucleation and growth over protein cages. *Langmuir* **2017**, *33*, 5925–5931.

(29) Lomonossoff, G. P.; Wege, C. *TMV Particles: The Journey From Fundamental Studies to Bionanotechnology Applications*; Academic Press Inc., 2018; Vol. 102; pp 149–176.

(30) Chu, S.; Brown, A. D.; Culver, J. N.; Ghodssi, R. Tobacco Mosaic Virus as a Versatile

Platform for Molecular Assembly and Device Fabrication. *Biotechnology Journal* **2018**, *13*, 1800147.

(31) Alonso, J. M.; Górzny, M. L.; Bittner, A. M. The physics of tobacco mosaic virus and virus-based devices in biotechnology. *Trends in Biotechnology* **2013**, *31*, 530–538.

(32) Klug, A. The tobacco mosaic virus particle: structure and assembly. *Philosophical Transactions of the Royal Society of London. Series B: Biological Sciences* **1999**, *354*, 531–535.

(33) Zahr, O. K.; Blum, A. S. Solution phase gold nanorings on a viral protein template. *Nano Letters* **2012**, *12*, 629–633.

(34) Bayram, S. S.; Zahr, O. K.; Re, J. D.; Blum, A. S. Nanoring formation via in situ photoreduction of silver on a virus scaffold. *Nanotechnology* **2016**, *27*, 485603.

(35) Zhou, K.; Zhang, J.; Wang, Q. Site-selective nucleation and controlled growth of gold nanostructures in tobacco mosaic virus nanotubulars. *Small* **2015**, *11*, 2505–2509.

(36) Dujardin, E.; Peet, C.; Stubbs, G.; Culver, J. N.; Mann, S. Organization of metallic nanoparticles using tobacco mosaic virus templates. *Nano Letters* **2003**, *3*, 413–417.

(37) Bromley, K. M.; Patil, A. J.; Perriman, A. W.; Stubbs, G.; Mann, S. Preparation of high quality nanowires by tobacco mosaic virus templating of gold nanoparticles. *Journal of Materials Chemistry* **2008**, *18*, 4796–4801.

(38) Iosin, M.; Baldeck, P.; Astilean, S. Study of tryptophan assisted synthesis of gold nanoparticles by combining UV–Vis, fluorescence, and SERS spectroscopy. *Journal of Nanoparticle Research* **2010**, *12*, 2843–2849.

(39) Yuan, H.; Khoury, C. G.; Hwang, H.; Wilson, C. M.; Grant, G. A.; Vo-Dinh, T. Gold nanostars: surfactant-free synthesis, 3D modelling, and two-photon photoluminescence imaging. *Nanotechnology* **2012**, *23*, 075102.

(40) Adigun, O. O.; Novikova, G.; Retzlaff-Roberts, E. L.; Kim, B. S.; Miller, J. T.; Loesch-Fries, L. S.; Harris, M. T. Decoupling and elucidation of surface-driven processes during inorganic mineralization on virus templates. *Journal of Colloid and Interface Science* **2016**, *483*, 165–176.

(41) Ahmad, N.; Wang, G.; Nelayah, J.; Ricolleau, C.; Alloyeau, D. Exploring the formation of symmetric gold nanostars by liquid-cell transmission electron microscopy. *Nano Letters* **2017**, *17*, 4194–4201.

(42) Kim, B. H.; Yang, J.; Lee, D.; Choi, B. K.; Hyeon, T.; Park, J. Liquid-phase transmission electron microscopy for studying colloidal inorganic nanoparticles. *Advanced Materials* **2018**, *30*, 1703316.

(43) Khelfa, A.; Nelayah, J.; Amara, H.; Wang, G.; Ricolleau, C.; Alloyeau, D. Quantitative in situ visualization of thermal effects on the formation of gold nanocrystals in solution. *Advanced Materials* **2021**, *33*, 2102514.

(44) Wu, H.; Friedrich, H.; Patterson, J. P.; Sommerdijk, N. A.; De Jonge, N. Liquid-Phase Electron Microscopy for Soft Matter Science and Biology. *Advanced Materials* **2020**, *32*, 2001582.

(45) Couasnon, T.; Alloyeau, D.; Ménez, B.; Guyot, F.; Ghigo, J.-M.; Gélabert, A. In situ monitoring of exopolymer-dependent Mn mineralization on bacterial surfaces. *Science Advances* **2020**, *6*, eaaz3125.

(46) Piffoux, M.; Ahmad, N.; Nelayah, J.; Wilhelm, C.; Silva, A.; Gazeau, F.; Alloyeau, D. Monitoring the dynamics of cell-derived extracellular vesicles at the nanoscale by liquid-cell transmission electron microscopy. *Nanoscale* **2018**, *10*, 1234–1244.

(47) Gnanasekaran, K.; Chang, H.; Smeets, P. J.; Korpanty, J.; Geiger, F. M.; Gianneschi, N. C. In situ Ni2+ stain for liposome imaging by liquid-cell transmission electron microscopy. *Nano Letters* **2020**, *20*, 4292–4297.

(48) Ambrožič, B.; Prašnikar, A.; Hodnik, N.; Kostevšek, N.; Likozar, B.; Žužek Rožman, K.; Šturm, S. Controlling the radical-induced redox chemistry inside a liquid-cell TEM. *Chemical Science* **2019**, *10*, 8735–8743.

(49) Schneider, N. M.; Norton, M. M.; Mendel, B. J.; Grogan, J. M.; Ross, F. M.; Bau, H. H. Electron–water interactions and implications for liquid cell electron microscopy. *The Journal of Physical Chemistry C* **2014**, *118*, 22373–22382.

(50) Alloyeau, D.; Dachraoui, W.; Javed, Y.; Belkahla, H.; Wang, G.; Lecoq, H.; Ammar, S.; Ersen, O.; Wisnet, A.; Gazeau, F., et al. Unravelling kinetic and thermodynamic effects on the growth of gold nanoplates by liquid transmission electron microscopy. *Nano Letters* **2015**, *15*, 2574–2581.

(51) Woehl, T. J.; Evans, J. E.; Arslan, I.; Ristenpart, W. D.; Browning, N. D. Direct in situ determination of the mechanisms controlling nanoparticle nucleation and growth. *ACS Nano* **2012**, *6*, 8599–8610.

(52) Ahmad, N.; Le Bouar, Y.; Ricolleau, C.; Alloyeau, D. Growth of dendritic nanostructures by liquid-cell transmission electron microscopy: a reflection of the electron-irradiation history. *Advanced Structural and Chemical Imaging* **2016**, *2*, 1–10.

(53) Woehl, T. J. Metal nanocrystal formation during liquid phase transmission electron microscopy: thermodynamics and kinetics of precursor conversion, nucleation, and growth. *Chemistry of Materials* **2020**, *32*, 7569–7581.

(54) Oster, G. The isoelectric points of some strains of tobacco mosaic virus. *J. Biol. Chem* **1951**, *190*, 55–59.

(55) Nedoluzhko, A.; Douglas, T. Ordered association of tobacco mosaic virus in the presence of divalent metal ions. *Journal of Inorganic Biochemistry* **2001**, *84*, 233–240.

(56) Bruckman, M. A.; Steinmetz, N. F. Chemical modification of the inner and outer surfaces of Tobacco Mosaic Virus (TMV). *Virus hybrids as nanomaterials: methods and protocols* **2014**, 173–185.

(57) Bayram, S. S.; Green, P.; Blum, A. S. Sensing of heavy metal ions by intrinsic TMV coat protein fluorescence. *Spectrochimica Acta Part A: Molecular and Biomolecular Spectroscopy* **2018**, *195*, 21–24.

TOC Graphic

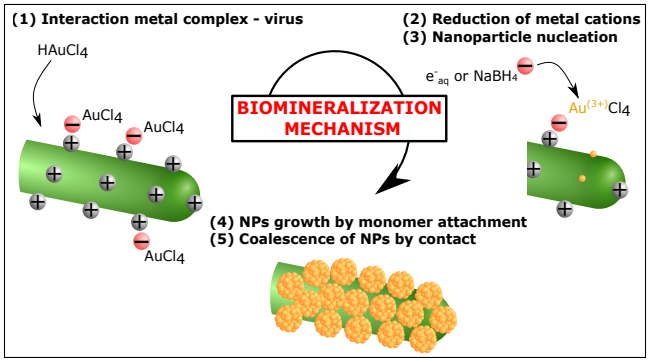
(1) Interaction metal complex - virus
(2) Reduction of metal cations
(3) Nanoparticle nucleation
HAuCl4
AuCl4
AuCl4
AuCl4
e-aq or NaBH4
Au(3+)Cl4
BIOMINERALIZATION MECHANISM
(4) NPs growth by monomer attachment
(5) Coalescence of NPs by contact